Theor Chem Account (2008) 120:565–573
DOI 10.1007/s00214-008-0423-x

REGULAR ARTICLE

Density functional studies of coinage metal nanoparticles: scalability of their properties to bulk

Alberto Roldán · Francesc Viñes · Francesc Illas · Josep Manel Ricart · Konstantin M. Neyman

Received: 13 November 2007 / Accepted: 6 February 2008 / Published online: 26 February 2008

Abstract Density functional plane-wave calculations have been carried out for series of Cu_n, Ag_n and Au_n particles containing up to 146 (Cu, Ag) and 225 (Au) atoms. Full geometry optimization has been performed for all particles starting from the structures created by cuts from the bulk. In line with previous studies, calculated average nearest-neighbour distances and cohesive energies of the particles linearly depend on such size-derived parameters as the average coordination number of metal atoms and the inverse of the mean particle radius, respectively. Rather accurate linear extrapolation of the observables under scrutiny to the bulk values has been achieved. However, we show that the scalability for particles made of various elements of the same $d^{10}s^1$ electron configuration differs, e.g. for bond lengths in Au_n species it is noticeably less perfect than that for Cu_n and Ag_n ones. Implications of encountered structural peculiarities of the nanoparticles for their reactivity are outlined.

Contribution to the Nino Russo Special Issue.

Electronic supplementary material The online version of this article (doi:10.1007/s00214-008-0423-x) contains supplementary material, which is available to authorized users.

A. Roldán · F. Viñes · F. Illas (✉) · K. M. Neyman
Departament de Química Física and Institut de Química Teòrica i Computacional (IQTCUB), Universitat de Barcelona, C/Martí i Franquès 1, 08028 Barcelona, Spain
e-mail: francesc.illas@ub.edu

A. Roldán · J. M. Ricart
Departament de Química Física i Inorgànica, Universitat Rovira i Virgili, C/Marcel.lí Domingo s/n, 43007 Tarragona, Spain

K. M. Neyman
Institució Catalana de Recerca i Estudis Avançats (ICREA), 08010 Barcelona, Spain

1 Introduction

The study of materials at the nanoscale constitutes a rather new and rapidly growing field with implications in industry and catalysis [1–3]. Industrial catalysts are often made of metal particles deposited on some kind of a support [4,5]. Information about how various properties change with size of the nanoparticles appears to be a very important issue. This includes, among other parameters, size-evolution of electronic and geometric structures and, for magnetic systems, also the evolution of magnetic moments. The ultimate goal behind the studies of size- and shape-dependent observables is the possibility to help to *tune* the reactivity and other particle parameters in a desired direction. One may think of designing metal nanoparticles with a special activity and selectivity towards a given reaction or prepare nanoparticles with particular electric or magnetic properties, which can be used as the basis for new devices.

There have been many experimental studies aimed at unravelling the structure of metal nanoparticles on different supports [6–11]. Several computational studies have also addressed these problems, although in most cases without directly taking the support into account [4,5,12–18]. A considerable effort has been devoted to predict the most stable isomers for a given transition metal nanoparticle of a certain (usually rather small) size; studies of the scalability of properties with the nanoparticle size are also reported [19–22]. As far as the shape is concerned, it has been demonstrated that three-dimensional (3D) metal crystallites cut from metal bulk by low-index planes are adequate starting models [23–29]. The latter provide a realistic representation of larger metal nanoparticles present in catalysts and offer some advantages with respect to the more conventional surface science models of two-dimensional (2D) extended surfaces, which lack atoms in a low coordination. In fact, it is well established

nowadays that low-coordinated metal atoms of stepped surfaces often exhibit a superior catalytic activity over those of ideal regular surfaces (e.g. [30–40] and references therein). For instance, it has been recently shown that low-coordinated atoms are crucial for the dissociation of molecular hydrogen on gold [41].

A realistic and appropriate representation of the nanoparticles involved in supported metal catalysts requires using 3D models in the regime when the properties are scalable (follow a monotonous trend) with increasing size, so that they eventually converge to the bulk values. The use of scalable models allows one to predict properties of larger particles of a realistic size without carrying out rather demanding calculations for them. However, there are two main problems when attempting to build models in the scalable regime. On the one hand, it is not quite clear how large the model particle under scrutiny needs to be to ensure scalability for a particular metal. On the other hand, these model particles can be too large to carry out state-of-the-art density functional (DF) calculations. Until recently, calculations on moderately large metal particles required dedicated codes, which efficiently handle symmetry [42,43]. Lately, it has been suggested to take advantage of the computational efficiency of codes that use plane-wave basis sets and translational symmetry. In this way DF calculations for nanoparticles containing up to ~200 metal atoms have been reported (see e.g., [22]). Moreover, one can utilize the periodic boundaries to study assembling of nanoparticles and even to model ordered superstructures [44].

In spite of the recent progress outlined above, there is almost no information about the scalable regime for metal nanoparticles other than Pd [20,21,23] and Au [19,20,22]. In this article we present an exhaustive systematic DF study of selected observables of nanoparticles of all three coinage metals and compare them with available results from previous studies. In particular, we focus on the convergence of mean interatomic distances and cohesive (binding) energies of Cu_n, Ag_n and Au_n nanoparticles towards the bulk values with increasing particle size. We also use this data set to re-assess precision of LDA (local-density approximation) and GGA (generalized-gradient approximation) functionals to quantify structural and energetic parameters of (heavy) metal systems.

2 Computational details

Density functional plane-wave calculations have been carried out with the help of VASP code [45–47] for three series of coinage metal particles M_n (M = Cu, Ag, Au), containing up to 225 atoms. The total energy was computed using either the LDA(VWN) [48] or the GGA(PW91) [49] exchange-correlation functionals. The effect of the core electrons on the valence electron density was described by the projector augmented wave (PAW) method [50,51]. The cut-off for the kinetic energy of the plane-waves has been set to 315 eV throughout, which ensures total energy convergence to better than 10^{-4} eV. A Gaussian smearing technique with a 0.2 eV width has been applied to enhance convergence but all energies presented in the following have been obtained by extrapolating to zero smearing (0 K). Smaller smearing values of 0.05 eV were employed to calculate DOS plots (see Sect. 3.3). Geometry optimization on selected starting geometries (see below) was carried out using a gradient-conjugate method until forces on all atoms were less than 0.3 eV/nm. Based on our test calculations, negligibly small spin-polarization effects were ignored throughout, except for spin-polarized energies of the atomic references. Both LDA and GGA functionals are considered to allow one a reasonably accurate description of (heavy) metallic systems (bulk, surfaces and clusters). In general, energies obtained at a GGA level are more precise but LDA is able to provide for such systems better geometries (see e.g. [19]). Therefore, we also performed calculations, in which the GGA energy was evaluated at the LDA geometry. Following the standard notation in molecular calculations, this approach is hereafter denoted as GGA//LDA. It has already proven to give accurate results for heavy metal systems [23,27 and references therein].

Single particles have been modelled by placing them into a large enough supercell, with a minimum vacuum space of 1 nm in all directions to avoid interactions between species in the neighbouring cells. This is a necessary requirement when using a plane wave basis set, which spans the whole space with the periodicity imposed by the unit cell chosen. However, to describe single particles it is sufficient to consider only the Γ-point of the reciprocal space. The centre of each particle has been placed at the unit cell centre. Cutting compact structures by low-index planes from the *fcc* metal bulk provided initial geometries for optimization. We studied coinage metal species M_n of both octahedral ($n = 44$, 85 and 146) and cuboctahedral shapes ($n = 38$, 55, 79, 116, 140, 147, 201 and 225; the latter three only for M = Au). Illustrative examples of Au_n nanoparticles are shown in Fig. 1. Note that geometry optimization always converged to a structure with the same topology, even though no symmetry constraints were imposed. It is worth emphasizing that no attempt has been made to find the most stable isomer for a given particle nuclearity, because our focus is on the properties scalability for particles of the *same fcc structural motif*.

All calculations have been carried out on parallel computers. Smaller M_n (M = Cu, Ag, Au; $n < 80$) moieties can be routinely calculated on a standard Linux cluster. However, for the larger species a supercomputer is required. In fact, LDA geometry optimization of the particles containing ~150 atoms typically takes ~4 CPU hours on 64 processors of

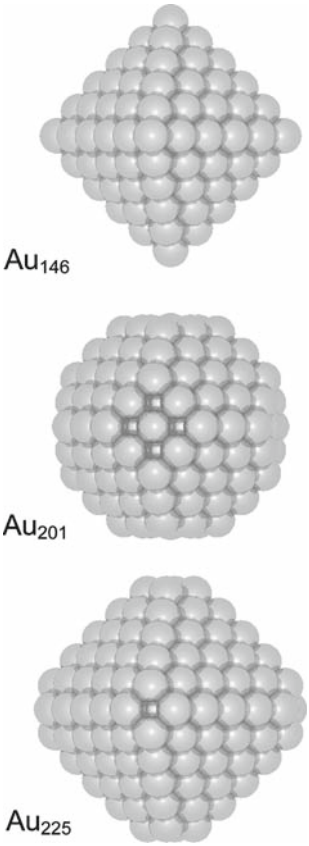

Fig. 1 Sketches of selected Au nanoparticles with octahedral (Au_{146}) and cuboctahedral (Au_{201}, Au_{225}) structures

the MARENOSTRUM supercomputer.[1] Therefore, rather time-consuming calculations for the clusters with 147, 201 and 225 atoms were carried out only for Au, assuming similar trends for the corresponding Cu and Ag particles.

3 Results and discussion

3.1 Geometric parameters

Interatomic distances in nanoparticles Cu_n, Ag_n and Au_n as well as the bulk values calculated at LDA and GGA levels are listed in Table 1 and compared with the experimental bulk distances [52–54]. Not unexpectedly [19,20], the LDA distances in all systems under scrutiny are shorter than the corresponding GGA values. Interestingly, differences of the average bond lengths d(GGA)–d(LDA) are not only substantial, ~8–10 pm, but also rather constant across the series of nanoparticles of different metals. Comparing the calculated and experimental bulk distances one observes overestimated d(GGA) values, deviations of which from experiment increase monotonously from just 2 pm for Cu, via 5 pm for Ag to 7 pm for Au. The latter overestimation is considerable, especially if compared to the precision of the d(LDA) value for Au bulk, exactly matching the experimental distance. The experimental distance for Ag bulk is just in the middle of the d(LDA)-d(GGA) interval and only for Cu does the GGA provide definitely superior accuracy for interatomic distances in coinage metal particles over the LDA distances. These results illustrate some practical consequences of the lack of a sufficiently accurate universal exchange-correlation functional (especially for heavy-element systems), which would be capable of equally precise description of the whole spectrum of observable parameters. We mention in the next section another implication of this problem—deficiencies in a consistent GGA description of the binding energy.

Let us focus on two other useful geometry indicators of the nanoparticles—minimum, $d_{\min}$, and maximum, $d_{\max}$, interatomic distances (Table 1). The difference $\Delta d = d_{\max} - d_{\min}$ increases smoothly from Cu_n to Au_n species of the same size and for the particles of the same metal with increasing size. For instance, Δd values for the particles with $n = 140$ and 146 increase from ~20 pm (Cu_n) and ~22 pm (Ag_n) to ~40 pm (Au_n); at GGA level $\Delta d(Au_n)$ values reach as much as 47 pm. This shows that Au_n particles differ significantly from the Cu_n and Ag_n analogues with respect to the $d_{\min}/d_{\max}$ distribution. Substantial size of Δd values, especially for larger particles considered, implies possibilities for noticeable alteration of the properties of atoms involved in the shortest and longest cluster M–M bonds, respectively. In general, the longest M–M bonds in the coinage metal particles are found for some of the surface atoms on (111) facets with some of their subsurface neighbours. It could be interpreted as a consequence of the surface stress that pushes outwards a small part of atoms exposed in the facets, thus leading to pronounced corrugation of the facets. Reactivity of such atoms with adsorbed species may well differ from that of their neighbours on the same facet. This effect should not be overlooked when comparing reactivity of nanoparticle facets with that of extended single-crystal surfaces.

In Fig. 2 we illustrate scaling of the average M–M bond distance d with the cluster size, expressed in terms of the average coordination number N_{av}. The latter is defined as a sum of the coordination numbers of all n atoms of a particle divided by n; for metal bulk $N_{\text{av}} = 12$ (data also included). Both LDA and GGA values are presented. In line with previous scalability studies for transition metal particles [19–21,23], the calculated average bond lengths converge rather rapidly to the corresponding bulk values, clearly manifesting development of the bulk character along each of the M_n series. On the other hand, these data reveal that even the largest nanocrystallite considered here, Au_{225} with its more than 60% of surface atoms and N_{av} value close to 80% of that for the bulk, is still not very close to the bulk limit, despite

[1] For details about the supercomputer architecture see www.bsc.es

Table 1 Average nearest-neighbour (d) and minimum/maximum (d_{min}/d_{max}, in parentheses) interatomic distances (in pm) of octahedral and cuboctahedral *fcc* Cu_n, Ag_n and Au_n particles of increasing size, characterized by average coordination numbers N_{av}, calculated using LDA(VWN) and GGA(PW91) functionals. The calculated and experimental metal bulk distances are also shown

n	N_{av}	Cu_n		Ag_n		Au_n	
		LDA	GGA	LDA	GGA	LDA	GGA
38	7.58	242 (239/251)	250 (247/260)	277 (273/288)	287 (284/298)	281 (273/309)	289 (281/316)
44[a]	7.64	243 (237/250)	251 (245/258)	278 (272/278)	288 (281/299)	280 (267/297)	288 (273/306)
55	7.85	243 (231/249)	251 (238/256)	278 (267/285)	288 (277/295)	280 (266/289)	289 (274/299)
79	8.51	244 (238/252)	252 (246/260)	280 (274/289)	290 (283/300)	283 (272/307)	292 (279/322)
85[a]	8.47	244 (234/251)	252 (242/261)	279 (268/288)	290 (278/300)	282 (268/302)	291 (274/314)
116	8.90	245 (237/252)	253 (244/260)	280 (271/288)	290 (282/297)	284 (268/316)	292 (275/329)
140	9.09	245 (237/257)	253 (244/266)	280 (272/294)	291 (282/306)	284 (272/312)	292 (279/326)
146[a]	9.04	245 (236/255)	253 (244/263)	280 (271/292)	291 (282/304)	284 (268/308)	292 (275/321)
147	8.98					283 (266/300)	291 (274/311)
201	9.43					284 (269/306)	292 (277/317)
225	9.49					284 (272/308)	293 (279/321)
Bulk	12.00	249	258	284	294	288	295
		256[b]		289[b]		288[b]	

[a] Octahedral starting geometry; cuboctahedral one for all other particles. The shape retained in symmetry-unrestricted optimized structures
[b] Experimental values from Refs. [52–54]

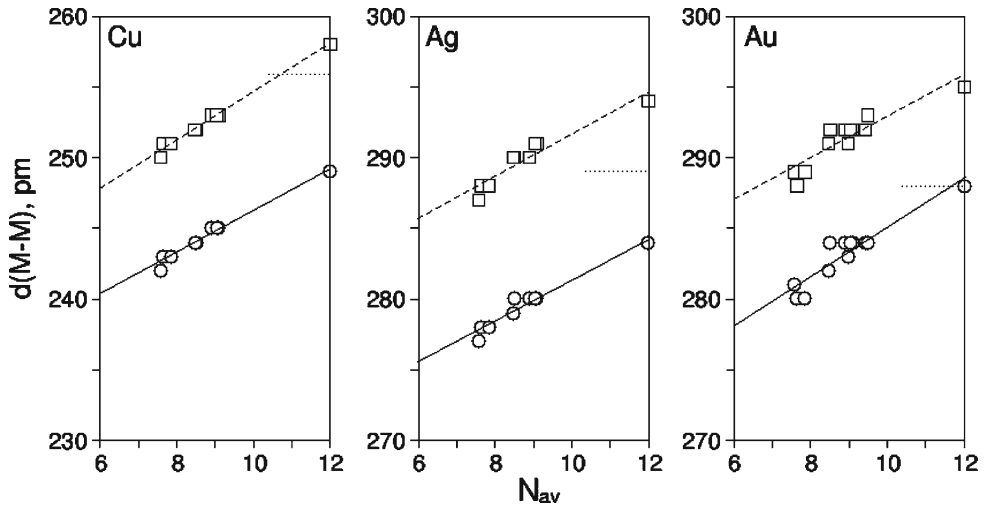

Fig. 2 Average nearest-neighbour interatomic distances d(M–M) of coinage metal (M = Cu, Ag, Au) particles M_n and bulk metals as a function of the average coordination number N_{av}. *Circles* and *solid lines* results of LDA(VWN) geometry optimization, *squares* and *dashed lines* correspond to GGA(PW91) geometry optimization. Experimental bulk values are also shown (*dotted lines*). Computed correlations for systems $38 \le n < \infty$(pm): $d^{Cu}(\text{LDA}) = 1.50 \times N_{av} + 231.4 (R^2 = 0.981)$, $d^{Cu}(\text{GGA}) = 1.70 \times N_{av} + 237.8 (R^2 = 0.996)$, $d^{Ag}(\text{LDA}) = 1.45 \times N_{av} + 266.9 (R^2 = 0.978)$, $d^{Ag}(\text{GGA}) = 1.42 \times N_{av} + 277.5 (R^2 = 0.948)$, $d^{Au}(\text{LDA}) = 1.75 \times N_{av} + 267.4 (R^2 = 0.940)$, $d^{Au}(\text{GGA}) = 1.51 \times N_{av} + 277.9 (R^2 = 0.825)$

the LDA and GGA d value is only 4 and 2 pm, respectively, or ~1% shorter than the corresponding bulk value.

One should mention that the correlations of d with N_{av} are linear with a rather high precision, especially for Cu_n and Ag_n. They give the values d extrapolated to the bulk to within 1 pm with respect to those explicitly calculated for the corresponding metal bulk. Interestingly, dispersion of the average distances d over the fitted lines is notably larger for Au_n systems than for other two coinage metals, in particular, at the GGA level. This clear manifestation of the worse scalability of interatomic distances for gold moieties with their size should probably be traced back to its strongly expressed relativistic character and partly related to its trend to form more open (planar) structures, compared to copper and silver

Table 2 Cohesive energy per atom (E_c, eV) of octahedral and cub-octahedral *fcc* Cu_n, Ag_n and Au_n particles of increasing size, $n \geq 38$, characterized by the inverse of the mean particle radius $R^{-1} \sim n^{-1/3}$, calculated using LDA(VWN) and GGA(PW91) functionals. Calculated and experimental values for the bulk metals are also shown

n	$n^{-1/3}$	Cu_n			Ag_n			Au_n		
		LDA	GGA	GGA//LDA	LDA	GGA	GGA//LDA	LDA	GGA	GGA//LDA
38	0.297	−3.54	−2.75	−2.71	−2.79	−1.98	−1.93	−3.38	−2.43	−2.38
44[b]	0.283	−3.55	−2.76	−2.72	−2.80	−1.99	−1.94	−3.44	−2.48	−2.43
55	0.263	−3.63	−2.82	−2.78	−2.87	−2.05	−2.00	−3.48	−2.51	−2.46
79	0.233	−3.76	−2.92	−2.87	−2.97	−2.11	−2.06	−3.62	−2.60	−2.55
85[b]	0.227	−3.76	−2.92	−2.88	−2.98	−2.11	−2.06	−3.63	−2.61	−2.56
116	0.205	−3.84	−2.98	−2.93	−3.04	−2.15	−2.10	−3.69	−2.64	−2.59
140	0.193	−3.91	−3.03	−2.99	−3.10	−2.20	−2.14	−3.76	−2.70	−2.65
146[b]	0.190	−3.90	−3.02	−2.98	−3.09	−2.19	−2.14	−3.76	−2.70	−2.65
147	0.189							−3.72	−2.67	−2.62
201	0.171							−3.83	−2.74	−2.69
225	0.164							−3.84	−2.75	−2.70
Bulk	0.000	−4.54	−3.52	−3.47	−3.63	−2.56	−2.49	−4.30	−3.06	−3.01
		−3.50[c]			−2.96[c]			−3.78[c]		

[a] LDA (GGA) notation means that the same LDA (GGA) functional is used both for geometry optimization and cohesive energy calculation; GGA//LDA notation specifies GGA energies calculated in a single point fashion for the LDA-optimized geometries
[b] Octahedral starting geometry; cuboctahedral one for all other particles
[c] Experimental values from Ref. [57]

[55,56]. Such peculiar structural behaviour of Au_n particles also implies that the onset of the scalable (to bulk) regime for them is postponed to larger sizes compared to congeners of the other two coinage metals, and, more generally, of other, less relativistic metals.

Finally, we compare our calculated interatomic distances with those of previous DF calculations [19,22], which were performed for smaller Au_n particles $n \leq 147$. Our average GGA bond-lengths d(Au–Au) of Au_n are very close, within 1 pm, to the values recently obtained using the same plane-wave computational technique [22]. However, unclear why d(Au–Au) = 292 pm has been calculated for Au bulk in Ref. [22], i.e. exactly equals to that in the four largest clusters Au_{116}, Au_{140}, Au_{146} and Au_{147} there. Note that our explicitly calculated bulk GGA distance d(Au–Au) is 295 pm, in full agreement with the value derived from our correlations. Probably, this inconsistency is related to the structure optimization approach of bulk gold, employed in Ref. [22]. Of special importance for such "relativistic" element as Au is benchmarking versus data of highly accurate all-electron scalar relativistic calculations [19]. The latter have been undertaken with O_h point-group symmetry and a DF code using Gaussian basis, similar to the code ParaGauss [42,43]. For the largest *fcc* cluster studied, Au_{55} [19], the LDA d(Au–Au) value with exactly the same exchange-correlation functional VWN as we used is 279 pm, i.e. only 1 pm shorter than in the present PAW plane-wave calculations. At GGA level (with a functional distinct from PW91 one used by us), the scalar relativistic d(Au–Au) = 287 pm [19] appears also to be in very good agreement with the presently calculated value of 289 pm having in mind notably different computational procedures employed. Average Au–Au bond lengths extrapolated to the bulk are in Ref. [19] even closer to the corresponding values of this work. Interestingly, both d(LDA) = 283 pm and d(GGA) = 291 pm values for the Au_{147} particle optimized under I_h symmetry constraints [19] match exactly the distances for the cuboctahedral Au_{147} particle (see Table 1).

3.2 Bonding energies

Cohesive (binding) energy per atom, E_c, is another important characteristic of nanoparticles. Our results are listed in Table 2, including calculated and experimental [57] values for bulk metals. Similarly to the interatomic distances, we computed and analysed bonding energies for the different particles at both LDA and GGA levels. In line with observations that GGA geometric parameters may appreciably deviate from accurate values, especially for heavy-element systems (see Sect. 3.1), we also examined performance of a combined GGA//LDA approach, according to which GGA energy is computed in a single-point fashion for the geometry optimized at LDA level. Beyond that one has at GGA//LDA level the opportunity to work with often more reliable geometries, such GGA//LDA calculations are faster, because instead

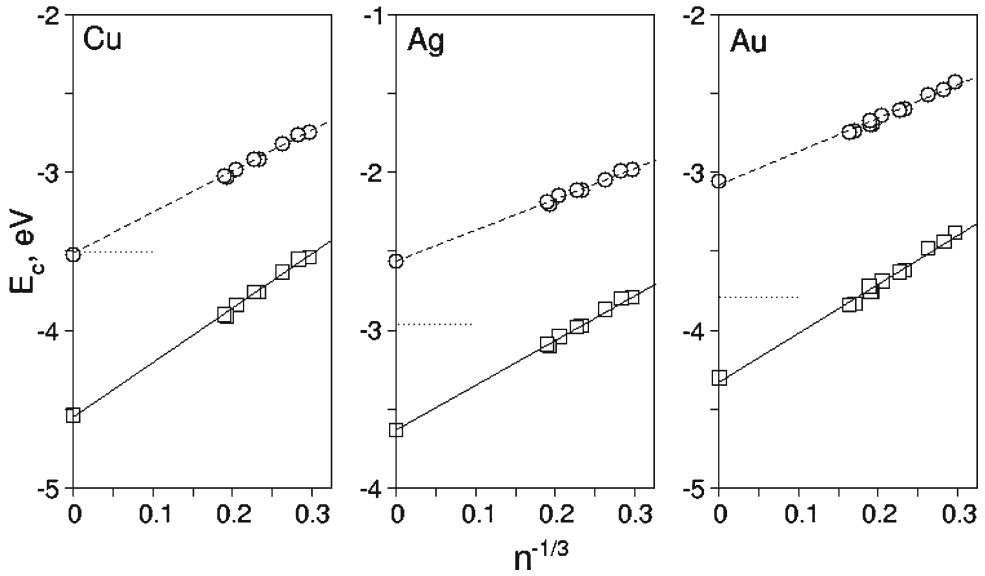

Fig. 3 Cohesive energy E_c (eV) per atom of coinage metal (M = Cu, Ag, Au) particles M_n and bulk metals as a function of the inverse of the mean particle radius $R^{-1} \sim n^{-1/3}$. *Circles* and *solid lines* LDA(VWN) energies, *squares* and *dashed lines* GGA(PW91) energies. Experimental bulk values are also shown (*dotted lines*). Computed correlations for $38 \leq n < \infty$: $E_c^{Cu}(\text{LDA}) = -4.548 + 3.446 \times n^{-1/3}$ ($R^2 = 0.997$), $E_c^{Cu}(\text{GGA}) = -3.552 + 2.643 \times n^{-1/3}$ ($R^2 = 0.997$), $E_c^{Ag}(\text{LDA}) = -3.631 + 2.870 \times n^{-1/3}$ ($R^2 = 0.998$), $E_c^{Ag}(\text{GGA}) = -2.565 + 1.978 \times n^{-1/3}$ ($R^2 = 0.997$), $E_c^{Au}(\text{LDA}) = -4.332 + 3.114 \times n^{-1/3}$ ($R^2 = 0.990$), $E_c^{Au}(\text{GGA}) = -3.087 + 2.128 \times n^{-1/3}$ ($R^2 = 0.986$)

of GGA geometry optimization less time-consuming LDA optimization is performed.

From calculated and experimental bulk values of cohesive energy (Table 2) a clear trend in the precision of the LDA and GGA emerges for metals along the group – Cu → Ag → Au. For Cu bulk E_c(GGA) = −3.52 eV quantitatively matches the experimental value of −3.50 eV [57], whereas at LDA the binding is much too strong, −4.54 eV. For Ag bulk, the presently used GGA PW91 furnishes binding energy of −2.56 eV, which notably, by 0.40 eV (14%), underestimates the experimental energy, −2.96 eV [57]. In fact, this rather low precision of GGA for Ag is of comparable size with that of LDA, which features overbinding by 0.67 eV. For Au, performance of GGA for the bulk binding energy is even worse, E_c(GGA) = −3.06 eV vs. experimental −3.78 eV [57], concomitantly, E_c(LDA) = −4.30 eV becomes somewhat closer to the experiment. These data illustrate that GGA in the form of one of the most widely used PW91 functional provides rather approximate description of the binding between heavy-element atoms, in particular 5d (Au) and, to lesser extend, 4d (Ag) metals. It appears to be a general deficiency of contemporary GGA functionals, not just of the PW91 one [27]. Therefore, the more economic and also often more accurate for geometric parameters combined GGA//LDA description of the metal binding energies may well be considered advantageous for the metals under scrutiny (Table 2): the deviation of E_c(GGA) from the corresponding E_c(GGA//LDA) energy is throughout close to ∼0.05 eV (∼5 kJ/mol), which is actually the best "chemical" accuracy that can be presently reached using DFT methods.

The binding per atom in M_n species is gradually strengthening with increasing particle size n, towards the corresponding energy in the bulk (Table 2). However, at variance with the interatomic distances, the binding energy per atom in the nanoparticles of the size considered here is still rather far from the bulk reference, reaching only ∼86% (Cu_{146}, Ag_{146}, Au_{146}) or 90% (Au_{225}) of the latter; the absolute particle-bulk energy deviation is quite significant and it ranges from ∼0.3 eV (Au) to ∼0.6 eV (Cu). E_c values of nanoparticles can be extrapolated to the bulk value as a function of the inverse of the mean particle radius R, approximated as $R^{-1} \sim n^{-1/3}$ [19–21,23]. Results of such extrapolations of the LDA and GGA energies calculated for the whole range of M_n clusters, $n \geq 38$, and including the calculated bulk value are shown in Fig. 3. Linearity of the fitted LDA and GGA energy correlations for all three series of metal systems is of rather high accuracy, as manifested by R^2 values close to 1 (see caption of Fig. 3). For most of the calculated E_c values the deviations from the respective fitted values are just ∼0.01 eV and only few outliers in the plots of Fig. 3 exhibit slightly larger deviations, limited to ∼0.05 eV. The energy correlations for Au, especially GGA one, are slightly less perfect than those for Cu and Ag, but the overall differences are much smaller than we have found for correlations of the interatomic distances (see Sect. 3.1). Thus, the specific character of relativistic metal Au with respect to Cu and Ag appears to manifest less

in the particle energetics than in the size-evolution of their M–M distances. Due to the still significant "gap" between the binding energies of computationally tractable moderately large metal particles and of the bulk, the presently derived sufficiently accurate correlations $E_c(n^{-1/3})$ should be useful for prediction of the binding strength for those coinage metal particles, which are still out of the scope of routine DF calculations.

Comparison of the present E_c(GGA) values for Au_n species ($n \leq 147$) with results of another VASP study [22] (introduced first as total energies of Au_n per atom, but subsequently compared with the E_c energies from Ref. [19]) reveals excellent agreement, with average energy deviations of ~0.01 eV. Only for Au_{116} was the value of −2.59 eV [22], 0.05 eV higher than E_c(GGA) = −2.64 eV that we obtained. However, if the energies from Ref. [22] are indeed total energies per atom, they would only fit our energies after a systematic offset by 0.15 eV—total spin-polarized PW91 energy of single Au atom. Interestingly, this offset brings the calculated total PW91 energy per atom for Au bulk, −3.20 eV [22], in perfect agreement with the corresponding present E_c value −3.06 eV (Table 2). Important finding is that our E_c(LDA) values for Au_n species (Table 2) in comparison with those for Au_{38}, Au_{44} and Au_{55} available from all-electron scalar relativistic calculations [19] agree basically quantitatively, with a systematic deviation of only ~0.05 eV, despite considerable differences in the two computational procedures. This justifies that even for such relativistic element as Au the present approximation of relativistic effects at the PAW VASP level is sufficiently reliable also for description of the Au–Au bond energies.

3.3 Electronic structure

Finally, we comment on the size dependence of the electronic structure of nanoparticles and how it approaches that of the bulk for all three studied coinage metals. We present and analyse the electronic structure in terms of the density of states (DOS). Note that the DOS peculiarities are responsible for major differences in the particle reactivity and thus could have very important implications for catalysis. Another aspect of even more general interest is how the bulk-like electronic properties are developed for nanoparticles of a particular metal when their size is increasing. In other words, the issue of interest is at which size range the particles start to behave not as large "molecules" with discrete electronic levels but rather as the smallest pieces of bulk featuring metallic electronic structure.

First we examined how the band smearing approximation of VASP (applied to converge electron density) affects the DOS plots. For that we compared DOS plots for Ag nanoparticles and bulk computed with the standard smearing of 0.20 eV (see Sect. 2) and reduced one of 0.05 eV. The results can be found in the Electronic Supplementary Material (ESM), in Fig. S1. For the bulk Ag and the largest particle Ag_{140} the effect of the smearing value is negligible and minor, respectively. However, for the smallest Ag_{38} species its molecular character is partially hidden when the smearing 0.20 eV is applied. So, we have chosen to plot all DOS with the smearing 0.05 eV. Also, characteristic features of DOS depend on the exchange-correlation functional. We studied this dependence for Ag_n particles and Ag bulk, by comparing DOS plots, positions of the d-band centre and numbers of states at the Fermi level calculated using GGA, GGA//LDA and LDA approaches; the comparison of GGA vs. GGA//LDA estimates the geometry uncertainty, whereas the GGA//LDA vs. LDA comparison (done for the same geometries) reveals a direct effect of the functional. Despite quantitative differences (see ESM, Fig. S2), trends in the DOS plots calculated at the GGA level appear to be representative. Thus, in the following we only discuss the GGA results.

In Fig. 4 GGA DOS plots for selected coinage metal nanoparticles M_n of increasing size (n = 38, 79, 140; M = Cu, Ag, Au) are compared to each other and to the plots for the bulk metals. Molecular character of all M_{38} species is clearly seen already at the first glance, for instance, from the quite extended regions of the zero DOS amplitude at the right-hand side of the energy scale; this is contrary to the essentially constant DOS values of bulk metals in these regions. In general, Fig. 4 manifests fast enough evolution of the DOS towards the bulk with increasing particle size. An important question is at which size the particles become sufficiently large, so that their DOS parameters monotonously approach those of the bulk. As an indicator of the DOS evolution with particle size we have chosen positions of the centre of valence d-bands, corresponding to the half of the cumulative d-projected density of states integrated till the Fermi level (see vertical arrows and numbers near them in Fig. 4). For all M_n species under scrutiny, starting from n = 79, this indicator goes monotonously with increasing n from the values for isolated atoms (not shown) down to the bulk values. On the other hand, the smallest members of the series, M_{38} species, do not follow this trend, in agreement with their above-mentioned molecular character. From this observation one can conclude that for coinage metal particles the onset of scalable-to-bulk properties (here, based on evolution of DOS parameters) requires about 80 atoms, similarly to what has been found for Pd nanoparticles based on the evolution of the adsorption properties [23]. Finally, DOS values per metal atom calculated for M_n species at the Fermi level E_f, also presented in Fig. 4, provide further evidence for the close similarity of the electronic structure of M_{140} particles and the bulk M as well as for noticeable differences with the electronic structure of M_{38} "molecules". However, this indicator of the electronic structure alteration appears to be less reli-

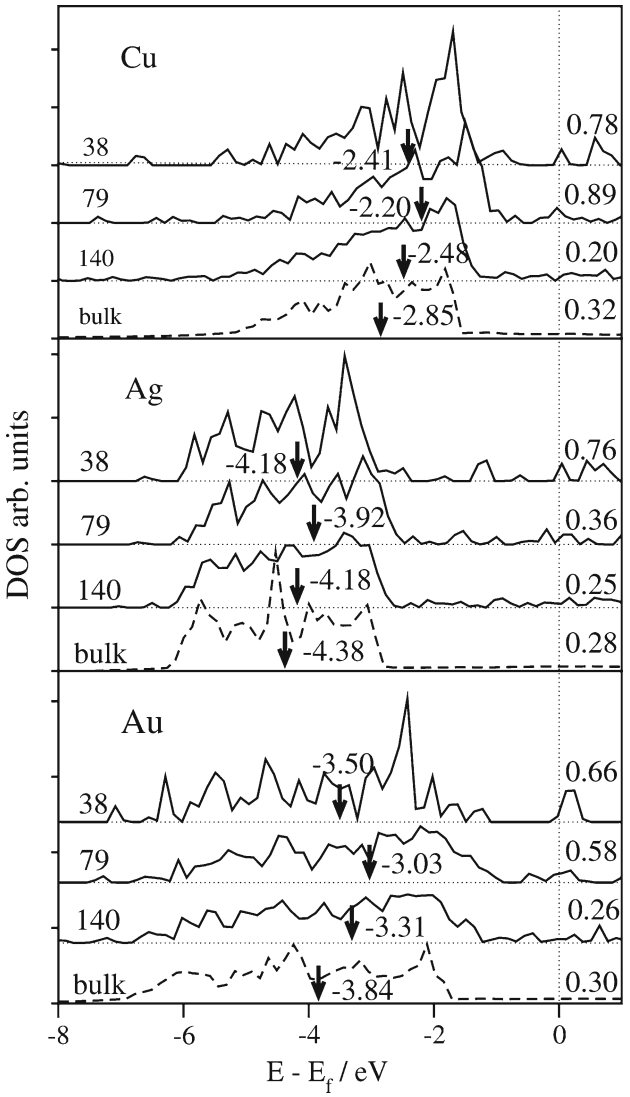

Fig. 4 GGA density of states (DOS) plots for selected coinage metal nanoparticles M_n of increasing size ($n = 38, 79, 140$; M = Cu, Ag, Au; *solid lines*) compared to the corresponding plot for bulk metal M (*dashed line*). *Arrows* and *numbers* near them indicate centres of the valence d-bands. DOS values per atom at the Fermi level E_f are also shown

able and characteristic than the just discussed centre of the d-band.

4 Summary and conclusion

Results of systematic density functional plane-wave calculations carried out for series of coinage metal particles containing up to 146 (Cu, Ag) and 225 (Au) atoms are presented. Full LDA and GGA geometry optimization has been performed for all particles starting from octahedral or cub-octahedral structures created by cuts from the metal bulk. Performance of the GGA, LDA and GGA//LDA schemes for the description of geometric and energetic parameters of the metal nanoparticles as well as trends along the group of the Periodic Table is critically evaluated. At variance with 3d metal Cu, GGA does not reveal definitely better accuracy than LDA for heavier 4d metal Ag and, especially, 5d congener Au. Applicability of the combined GGA//LDA scheme is corroborated. In line with previous studies (mainly of Pd and Au nanoparticles), calculated average nearest-neighbour distances and cohesive energies of the particles are found to depend linearly on such size-derived parameters as the average coordination number of metal atoms and the inverse of the mean particle radius, respectively. Rather accurate linear extrapolation of the observables under scrutiny to the bulk values has been achieved. However, the scalability for particles made of various elements of the same $d^{10}s^1$ electron configuration differs, e.g. for bond lengths in Au_n species it is noticeably less perfect than in case of Cu_n and Ag_n. The correlations established in this work allow one to quantitatively predict binding energies of coinage metal nanoparticles filling the gap between the currently computationally tractable particles of up to 100–200 atoms and larger ones, parameters of which more closely approach the bulk ones. Particle electronic structure evolution towards the bulk with their increasing size has been discussed; we show that in order for the DOS parameters start to be scalable to those of the bulk the particles should contain about 80 or more coinage metal atoms. Implications of detected structural peculiarities of the nanoparticles for their reactivity are outlined. Especially important for future applications of the plane-wave approach is an excellent agreement of the present interatomic distances and the binding energies of Au_n particles with data of previous benchmark all-electron scalar relativistic calculations. Among advantages of the present plane-wave approach is its applicability in an almost routine fashion and without symmetry restrictions to realistically mimic crystallites present in metal catalysts and their reactivity.

Acknowledgments This article is dedicated to Prof. Nino Russo in the occasion of his 60th birthday. FV and AR thank the Spanish Ministry of Education and Science (MEC) and Universitat Rovira i Virgili, respectively, for supporting their pre-doctoral research. Financial support has been provided by the MEC (grants CTQ2005-08459-CO2-01, CTQ2005-08459-CO2-02, UNBA05-33-001, HA2006-0102) and the Generalitat de Catalunya (2005SGR00697, 2005SGR-00104, 2005 PEIR 0051/69 and *Distinció per a la Promoció de la Recerca Universitària* granted to FI). Computational time on the *Marenostrum* supercomputer of the Barcelona Supercomputing Center is gratefully acknowledged.

References

1. Daniel MC, Astruc D (2004) Chem Rev 104:293–346
2. Lambert RM, Pacchioni G (eds) (1997) Chemisorption and reactivity on supported clusters and thin films. Towards an understanding

of microscopic processes in catalysis, NATO ASI Series Kluwer, Academic Publishers, Dordrecht
3. Bäumer M, Freund HJ (1999) Progr Surf Sci 61:127–198
4. Fernandez-Garcia M, Anderson JA (eds) (2005) Supported metals in catalysis, Catalytic sciences series, vol. 5, Imperial College Press, London
5. Wieckowski A, Savinova E, Vayenas CG (eds) (2003) Catalysis and electrocatalysis at nanoparticle surfaces. Marcel Dekker, New York
6. Maeda Y, Okumura M, Tsubota S, Kohyama M, Haruta M (2004) Appl Surf Sci 222:409–414
7. Wang CM, Shutthanandan V, Zhang Y, Thevuthasan S, Thomas LE, Weber WJ, Duscher G (2006) Nucl Instr Meth Phys Res B 242:380–382
8. Pakarinen OH, Barth C, Foster AS, Nieminen RM, Henry CR (2006) Phys Rev B 73:235428 (1–10)
9. Min BK, Wallace WT, Goodman DW (2006) . Surf Sci 600:L7–L11
10. Akita T, Okumura M, Tanaka K, Kohyama M, Haruta M (2005) J Mater Sci 40:3101
11. Boyen H-G, Herzog Th, Kästle G, Weigl F, Ziemann P, Spatz JP, Möller M, Wahrenberg R, Garnier MG, Oelhafen P (2002) Phys Rev B 65:075412 (1–5)
12. Wilson NT, Johnston RL (2002) J Mater Chem 12:2913–2922
13. Ascencio JA, Liu HB, Pal U, Medina A, Wang ZL (2006) Microsc Res Tech 69:522–530
14. Ricci D, Bongiorno A, Pacchioni G, Landman U (2006) Phys Rev Lett 97:036106 (1–4)
15. McKenna KP, Sushko PV, Shluger AL (2006) J Chem Phys 126:154704 (1–9)
16. Yang X, Cai W, Shao X (2007) J Phys Chem A 111:5048–5056
17. Xiao L, Tollberg B, Hu X, Wang L (2006) J Chem Phys 124:114309 (1–10)
18. Aprà E, Ferrando R, Fortunelli A (2006) Phys Rev B 73:205414 (1–5)
19. Häberlen OD, Chung SC, Stener M, Rösch N (1997) J Chem Phys 106:5189–5201
20. Krüger S, Vent S, Rösch N (1997) Ber Bunsenges Phys Chem 101:1640–1643
21. Krüger S, Vent S, Nörtemann F, Staufer M, Rösch N (2001) J Chem Phys 115:2082–2087
22. Barnard AS, Curtiss LA (2006) Chem Phys Chem 7:1544–1553
23. Yudanov IV, Sahnoun R, Neyman KM, Rösch N (2002) J Chem Phys 117:9887–9896
24. Yudanov IV, Sahnoun R, Neyman KM, Rösch N, Hoffmann J, Schauermann S, Johánek V, Unterhalt H, Rupprechter G, Libuda J, Freund HJ (2003) J Phys Chem B 107:255–264
25. Yudanov IV, Neyman KM, Rösch N (2004) Phys Chem Chem Phys 6:116–123
26. Neyman KM, Sahnoun R, Inntam C, Hengrasmee S, Rösch N (2004) J Phys Chem B 108:5424–5430
27. Neyman KM, Vayssilov GN, Rösch N (2004) J Organomet Chem 689:4384–4394
28. Neyman KM, Inntam C, Gordienko AB, Yudanov IV, Rösch N (2005) J Chem Phys 122:174705 (1–9)
29. Yudanov IV, Neyman KM, Rösch N (2006) Phys Chem Chem Phys 8:2396–2401
30. Taylor HS (1925) Proc R Soc A 108:105–111
31. Dahl S, Logadottir A, Egeberg RC, Larsen JH, Chorkendorff I (1999) Phys Rev Lett 83:1814–1817
32. Dahl S, Tornqvist E, Chorkendorff I (2000) J Catal 192:381–390
33. Wolf RM, Bakker JW, Nieuwenhuys BE (1991) Surf Sci 246:135–140
34. Zambelli T, Wintterlin J, Trost J, Ertl G (1996) Science 273:1688–1690
35. Banholzer WF, Masel RI (1984) J Catal 85:127–134
36. Klier K, Hess JS, Herman RG (1997) J Chem Phys 107:4033–4043
37. Uhara I, Kishimoto S, Yoshida Y, Hikino T (1965) J Phys Chem 69:880–882
38. Jia J, Haraki K, Kondo JN, Domen K, Tamaru K (2000) J Phys Chem B 104:11153–11156
39. Uetsuka H, Watanabe K, Kimpara K, Kunimori K (1999) Langmuir 15:5795–5799
40. Gonzalez S, Loffreda D, Sautet P, Illas F (2007) J Phys Chem C 111:11376–11383
41. Corma A, Boronat M, González S, Illas F (2007) Chem Comm 3371–3373
42. Belling T, Grauschopf T, Krüger S, Mayer M, Nörtemann F, Staufer M, Zenger C, Rösch N (1999) High performance scientific and engineering computing. In: Bungartz H-J, Durst F, Zenger C (eds) Lecture notes in computational science and engineering. Springer, Heidelberg vol 8, p 439
43. Belling T, Grauschopf T, Krüger S, Nörtemann F, Staufer M, Mayer M, Nasluzov VA, Birkenheuer U, Hu A, Matveev AV, Shor AM, Fuchs-Rohr MSK, Neyman KM, Ganyushin DI, Kerdcharoen T, Woiterski A, Gordienko AB, Majumder S, Rösch N (2004) PARAGAUSS, Version 3.0, TU München
44. Viñes F, Illas F, Neyman KM (2007) Angew Chem Int Ed 46:7094–7097
45. Kresse G, Furthmüller J (1996) Comp Mat Sci 6:15–50
46. Kresse G, Hafner J (1993) Phys Rev B 47:558–561
47. Kresse G, Furthmüller J (1996) Phys Rev B 54:11169–1186
48. Vosko SH, Wilk L, Nusair M (1980) Can J Phys 58:1200–1211
49. Perdew JP, Wang Y (1992) Phys Rev B 45:13244–13249
50. Blöchl PE (1994) Phys Rev B 50:17953–17979
51. Kresse G, Joubert D (1999) Phys Rev B 59:1758–1775
52. CRC Handbook of Chemistry and Physics (1983) Weast RC (ed), 64 ed, CRC Press, Boca Raton FL
53. Wang L, Cheng H (2004) Phys Rev B 69:045404 (1–7)
54. Wang L, Cheng H (2004) Phys Rev B 69:165417 (1–12)
55. Häkkinen H, Moseler M, Landman U (2002) Phys Rev Lett 89:033401 (1–4)
56. Dong Y, Springborg M (2007) J Phys Chem C 111:12528–12535
57. Kittel C (1956) Introduction to solid state physics. Wiley, New York